Journal of Polymer Research (2021) 28: 445
https://doi.org/10.1007/s10965-021-02804-7

ORIGINAL PAPER

Fabrication of starch-based multi-source integrated halogen-free flame retardant in improving the fire safety of polypropylene

Zaihang Zheng[1,2] · Yurou Xia[1] · Chenchen Liao[1] · Yuhang Liu[1] · Weihong Chai[1] · Enchen Niu[1] · Ziqing Hu[1]

Received: 17 May 2021 / Accepted: 20 October 2021 / Published online: 29 October 2021

Abstract

Aimed at increasing the fire safety of polypropylene (PP), starch-based and green flame retardant (SSPM) have been prepared. Additionally, the employment of starch as bio-based char-forming materials was aimed at replacing the petroleum-based, expensive and unsustainable carbon source. Thermal degradation tests demonstrated that as-prepared SSPM possessed good thermal expansion properties with 44.7% char residue at 600 °C. When 30 phr SSPM was added to PP by melting blending process, PP composites can acquire 26.4% LOI value and UL-94 V-1 rating. Through analyzing the thermal degradation process, the promotion effect of SSPM in char-formation was obtained. Further research on char residue has initially proposed a potential flame retardant mechanism. Therefore, this paper provided a new bio-based route in replacing the petroleum-based char source for decreasing the fire risk of PP materials in actual life.

Keywords Starch · Bio-based · One-component · Flame retardant · Intumescent · Polypropylene

Introduction

As the general polymer, polypropylene (PP) has many advantages, such as low production cost, good mechanical properties, non-toxicity, light weight, corrosion resistance, good electrical performance, easy processing and easy recycling, etc. [1–3]. Therefore, PP shows broad applications in fields of packaging, textiles, architecture, automobiles, electronics, electrics, office supplies and daily necessities. Unfortunately, PP is inflammable that will produce lots of droplets and diffused flame [4–7]. This fatal defect seriously deteriorates the more widespread application of PP materials. With the growing demands of PP materials, the potential fire risks increase. Therefore, improving the flame retardancy of PP materials have become an urgent problem. Thus, many researchers have paid enormous effort on solving flammability for PP materials. In the past several decades, halogen-containing flame retardants had once occupied the most critical position for polyolefins because of its high efficiency. But their high toxicity and corrosive gases production will cause extreme environment and human health problem. As the eco-friendly and low-cost materials, halogen-free flame retardants have gradually turn into the development trend in recent years [8–10]. During these, intumescent flame retardants (IFR) are excellent candidates on account of smoke reduction, non-toxic and non-corrosive gas release [11–13]. In the 1980s, Camino et al. have conducted many pioneering works and the P-N synergistic theory was established [14, 15]. Generally, this system are composed of three parts: catalysts, char source and blowing agents. During the combustion of PP, the generation of inert gases from blowing agent can dilute the concentration for combustible gases and oxygen. Simultaneously, the esterification reaction between catalysts and char source can produce the uniform porous char foam that can action in heat insulation, oxygen isolation, smoke suppression and melting resistance [16]. Thereby, this imparts excellent efforts for flame-retarding PP. Conspicuously, char source quality will directly determine the flame retardant effect. Most of char sources are polyhydroxy-containing compounds produced by petroleum cracking, such as pentaerythritol (PER) and its derivatives [17]. However, the excessive consumption of energy can cause the serious environmental pollution. Thus, people have gradually turned their attention to the

✉ Zaihang Zheng
zhengzaihang@ccut.edu.cn

[1] School of Chemical Engineering, Changchun University of Technology, Changchun 130012, P. R. China

[2] Key Laboratory of Bionic Engineering (Ministry of Education), Jilin University, Changchun 130022, P. R. China

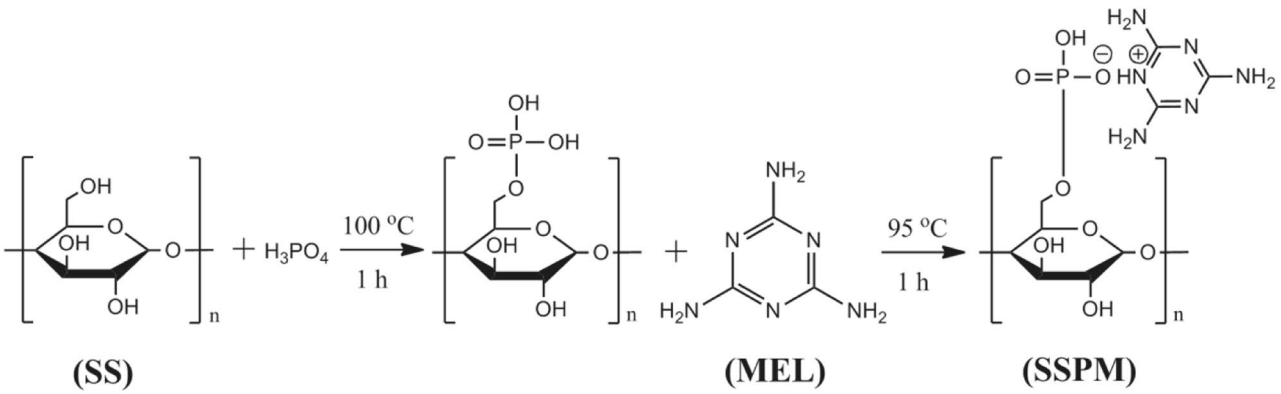

Scheme 1 Illustration for fabricating SSPM

bio-based materials [18]. Among these, Passauer has utilized starch derivatives (SPC) as the green char-forming agent. Activation temperatures of SPC markedly decreased with increasing DS that were considerably lower than decomposition temperatures of pure starch. The ammonia releasing from thermal degradation of SPC was identified to flame extinguishment. Therefore, SPC becomes the promising candidates for sustainable and eco-friendly flame-retardants [19]. Moreover, Xu et al. have designed the alginate pillared hydrotalcite (SA@LDHs) in order to improve the flame retardancy for PP composites. The PP/30 wt%SA@LDHs achieved 30.9% LOI value and UL-94 V-0 rating. Compared with neat PP, the peak heat release rate, total heat release and total smoke production of PP/SA@LDHs were greatly decreased. The tests demonstrate that the radical-trapping effect of SA leads to the prominent increase for fire safety [20]. In our previous work, a bio-based flame retardant with 43% char residue at 600 °C has also been fabricated. When blended with expandable graphite, PP composites can acquire 31.5% LOI value and UL-94 V-0 rating. All of facts have revealed positive effect of bio-based char-forming agent [21].

As we know, starch is a natural polysaccharide formed by shrinking a plurality of glucose units via photosynthesis of plants. Starch is widely used in textile, petroleum exploitation, feeds and food industries due to its rich source and low price. Due to the polyhydric groups, starch can form char barrier in flame retardant process. Therefore, the use of starch is expected as one of green char source candidates [22]. In this paper, aiming at improving the fire safety of PP, a starch-based integrated flame retardant (SSPM) was constructed. The chemical structure, surface morphology and thermal stability of SSPM were characterized by Fourier transform infrared spectroscopy (FTIR), scanning electron microscopy (SEM) and thermogravimetric analysis (TGA). In addition, the flame retardancy of PP composites were tested by limited oxygen index (LOI), vertical burning tests (UL-94) and cone calorimeter tests (CCT), respectively. On account of the systematic analysis on char residue, the flame retardant mechanism of bio-based compounds in PP has been illustrated.

Experimental

Materials

Polypropylene (PP) was purchased from by China Petrochemical Co. Ltd. Concentrated phosphoric acid (85 wt%) was acquired in Beijing Chemical Works. Starch soluble (SS) has been procured via Tianjin Tiantai Co., Ltd. Melamine was originated from Tianjin Yongsheng Co., Ltd. The deionized water was prepared in our lab.

Fabrication of starch-based compound

As presented in Scheme 1, 5 g soluble starch was mixed with 15 mL concentrated phosphoric acid under magnetically stirring until the solution was in a transparent state. The concentrated phosphoric acid solution of soluble starch was transferred to a Teflon-lined stainless steel reactor, and placed in a 100 °C drying oven for 1 h to obtain a yellow liquid as a flame retardant intermediate (starch soluble phosphate, SSP). After that, the melamine was ultrasonically dispersed in a 250 mL three-necked flask by adding 100 mL of deionized water to prepare a melamine aqueous dispersion. The melamine aqueous dispersion was transferred to a three-necked flask with mechanically stirring. When heated to 95 °C, the flame retardant intermediate was dropwise added into the flask. Until this process was complete, the reaction was kept at a constant temperature for another 1 h. When the system is cooled to room temperature, the obtained moist product was obtained via filtrating under vacuum and rinsing by hot water for 3–5 times. Finally, starch-based one-component three-source integrated

compound (SSPM) has been gained after dried at 80 °C overnight and mechanical grinding.

Melt blending process

Based on Table 1, all materials have been blended via HAAKE Rheodrive torque theometer (manufactured by Thermo Fisher Scientific, HAAKE PolyLab OS RheoDrive 7) at 180 °C for 7 min. The rotating speed was set as 60 rpm. Then, samples have been separately compressed and obtained at 190 °C temperature and 10 MPa pressure for 10 min.

Measurements and characterization

Infrared spectroscopy (FTIR)

Sample was prepared by the potassium bromide tableting method. The composition of the samples was analyzed using a Nicolet IS10 FT-IR spectrometer from Thermo Fisher Scientific. The infrared spectrum ranges from 500 to 4000 cm^{-1} with 32 scans and a resolution of 4 cm^{-1}.

Scanning Electron Microscopy (SEM)

Microscopic state of solid samples were observed via a JSM-6510 equipment (JEOL, Japan). Before tests, samples have been electroplated by Au.

Thermogravimetric Analysis (TGA)

Before experiments, specimens must be maintained at 100 °C for 24 h. The curves of specimens were acquired via the PerkinElmer STA6000 Synchronous Thermal Analyzer at N_2 atmosphere. The test temperature was from 50 °C to 750 °C at a heating rate of 10 °C/min. The weights of samples were about 10 mg. Differential thermo-gravimetric curves (DTG) were obtained by calculating the integral curve of TGA plots. Except that, the fitting curves have been achieved via linear percentage addition of mixture components.

$$W_{cal}(T) = \sum_{i=1}^{n} xiWi(T)$$

Here, x_i presents "component i" percentage; W_i presents "component i" curve.

Limiting Oxygen Index (LOI)

In this paper, LOI values have been obtained via GBT2406 equipment (Suzhou Difansi Co., Ltd) on account of ASTM D 2863–97. The samples size have been set as $(120–130) \times 10 \times 3$ mm^3. During tests, the threshold value of samples was set as 3 min flame time or 50 mm combustion length. In the case of exceeding 3 min flame time or 50 mm combustion length, samples's LOI value should be decreased. On the contrary, in the case of exceeding 3 min flame time or 50 mm combustion length, samples' LOI value should be increased. Besides, the test accuracy was ± 0.1% via three parallel experiments.

UL-94 tests

UL-94 tests were conducted by XD-B46 equipment (Dongguan Xudong Co., Ltd.) on the basis of international standard. And the samples' size was set as $130 \times 13 \times 3$ mm^3.

Combustion calorimeter tests

Cone calorimeter tests (Stanton Redcroft, UK) were performed according to ISO 5660 standard. The specimens with dimensions $100 \times 100 \times 3$ mm^3 were put on a horizontal aluminum tray and exposed horizontally to an incident under 35 kW/m^2 heat flux.

Mechanical tests

Young's modulus, tensile strength and elongation at break were measured according to ASTM D638 standard with a 3365 Instron universal tensile testing machine. The specimens were prepared according to the same standard. Crosshead speed was set as 50 mm/min. The values of mechanical properties were obtained by calculating the results of at least five specimens tests.

X-ray photoelectron spectroscopy (XPS)

In this paper, XPS spectra employed to investigate the surface elements via VG ESCALABMK type equipment (UK).

Table 1 The detailed formulation and flame retardant tests results of PP composites

Sample	PP phr	SS phr	SSPM phr	LOI %	UL-94	Dripping
PP	100	-	-	17.0	NR	Yes
PP/SS	100	30	-	21.7	NR	Yes
PP/SSPM	100	-	30	26.4	V-1	No

Results and discussions

Chemical structure

In order to detect the chemical structure of SS and SSPM, the FTIR spectra were employed, as shown in Fig. 1a. As for SS, the absorption peaks appearing around 3138 cm^{-1} and 2925 cm^{-1} are mainly asymmetric stretching vibrations of the -OH groups and the -CH_2 groups [23]. And the absorption peaks near 1158 cm^{-1} and 1048 cm^{-1} are assigned to the stretching vibration of the C-O groups in the molecular chains of SS [23]. After the reaction, the FTIR spectrum of SS was significantly changed. Obviously, the absorption peak at 3407 cm^{-1} can be attributed to amino (N–H) structure [24]. Furthermore, absorption located in 1670, 1517 and 1331 cm^{-1} may be caused by the nitrogen–hydrogen structure and the typical triazine ring structure of melamine [25]. In addition, absorption appeared in 1048, 958 and 1245 cm^{-1} can be assigned to phosphorus-oxygen groups [26]. Thus, the FTIR spectrum of SSPM not only contains the characteristic peaks containing melamine but also the characteristic groups of phosphoric acid. The results show that the phosphoric acid and melamine have been introduced onto the structure of SS by the chemical interaction to some extent.

Moreover, aiming at better understanding the chemical structure, XPS spectra of SS and SSPM were also acquired for analysis. Generally, XPS spectra could offer more surface elements' evidence on the composition structure. Apparently, SS contains carbon and oxygen elements with the percentage of 64.48% and 26.62% in Fig. 1b. For SSPM, the new peaks appears at 133.6 eV, 191.5 eV and 400.1 eV that are assigned to the P2p, P2s and N1s [27, 28]. And the N and P contents on the surface of SSPM are 28.75% and 6.89% that reflect the loading of phosphoric acid and MEL in the structure of SS to some extent. Therefore, we can conclude that the changes in the XPS spectra of SS and SSPM are attributed to the successful synthesis of starch-based halogen-free intumescent flame retardants. This result can further replenish the conclusion of FTIR spectra.

Surface morphology

Microscopic state of SS and SSPM has been acquired via scanning electron microscopy. Figure 2 has revealed that surface of the starch granules is smooth, and the large typical granules are shaped like potato tubers with no fixed shape. The small particles are approximate oval, and the immature small granules are spherical. The apparent size of the starch granules is about 10–75 μm. For SSPM, the surface morphology of SSPM was observed to be very different from SS after the chemical reaction among SS, phosphoric acid and MEL. The phosphorus-nitrogen-containing compound has a distinct monoclinic structure with hexagonal ends and rough surface. In addition, SSPM has an apparent size of about 50–100 μm, which is slightly larger than starch. This change in surface morphology can also reveal the formation of SSPM to a certain degree.

Thermal decomposition

Thermal stability is one of the most important properties for flame retardants. The thermal decomposition condition

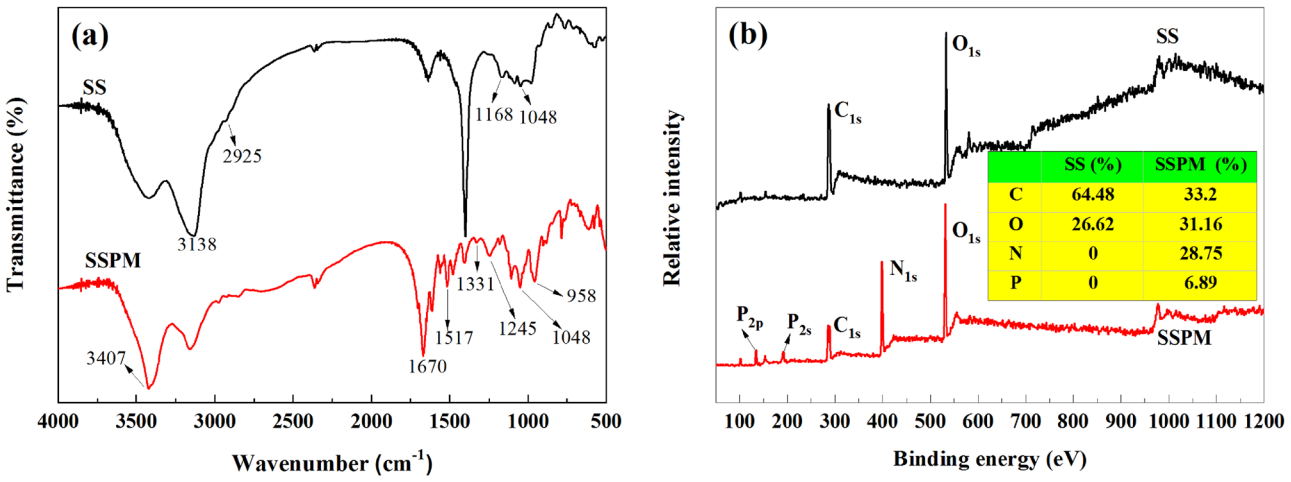

Fig. 1 Chemical structure of SS and SSPM, (**a**) FTIR spectra, (**b**) XPS spectra

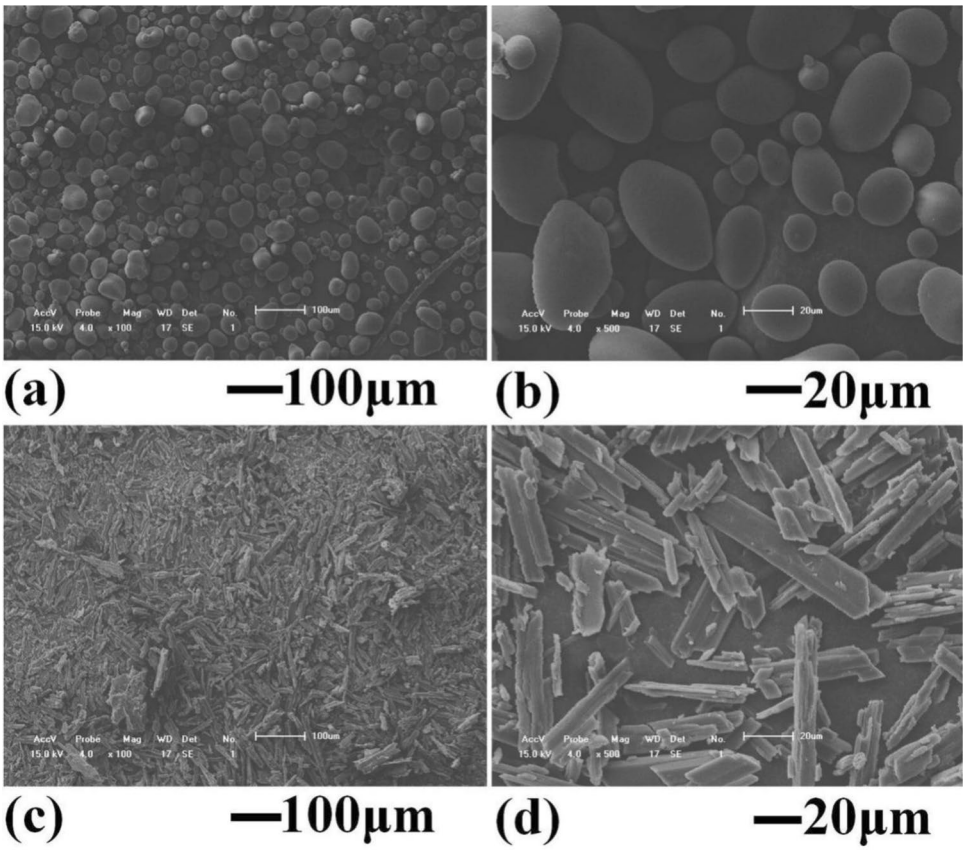

Fig. 2 Microscopic structure: (**a**–**b**) SS, (**c**–**d**) SSPM

for SS and SSPM has been evaluated via thermogravimetric analysis (TGA) in Fig. 3. In addition, the tests also show the derivative thermogravimetry (DTG) of the TGA curve. Generally, thermogravimetric analysis is one of the important methods for investigating the thermo-degradation state for powder and polymer. It can be seen that the thermal decomposition process of starch are divided into two weight-loss steps. The decomposition temperature (5% weight loss temperature, $T_{5\%}$) for first weight loss process was around 250–330 °C, and the weight loss of starch was 13.6%. At this stage, the rapid dehydration and decomposition of the hydroxyl groups in glucose rings will form water molecules. At the same time, the C–C-H, C-O and C–C bonds in starch are thermally broken and the main decomposition products are H_2O, CO, CO_2 and some hydrocarbon compounds (CH_4 and C_2H_4) [23]. And the second weight loss process concentrates at 250–400 °C. The char residue of the starch is 8.61% at 800 °C. As for SSPM, the $T_{5\%}$ value is significantly lower than SS. And SSPM shows a multi-step thermal degradation process. The two weight loss peaks in the temperature range of 261–345 °C are ascribed to the initial degradation of starch and the sublimation of melamine, as presented in Fig. 3b. At a temperature range of 345–600 °C, the SSPM is further decomposed while the dehydration esterification reaction between phosphoric acid domains and melamine domains occurs. When the temperature reaches 600 °C, the residual rate of SSPM reaches 44.7%, which is much higher than the starch. This is beneficial to form the barrier layer for heat during combustion and improve the flame retardant efficiency of SSPM in PP. As shown in Fig. 3b, the decomposition rate of the starch reached a maximum at 300 °C, while the maximum decomposition rate of SSPM reached 400 °C. In addition, the obvious thermal expansion phenomenon appears after heated at 600 °C, which is originated that inert gas release from the melamine domains in the SSPM to promote the formation of a dense expanded char layer during heat, as shown in Fig. 3d. Therefore, this heated intumescence and char-forming process of SSPM will be dominant in view of decreasing flame risk. The detailed changes in chemical and morphology structure of SSPM have been discussed as follows.

Thermal oxidative process analysis of SSPM

The carbonaceous process of the starch-based flame retardant was studied by FTIR spectra to detect the flame retardant char residue obtained at different temperatures. The SSPM was heated in a muffle furnace in an air atmosphere at a heating rate of 10 °C/min. The flame retardant powder was heated to different temperature and separately held

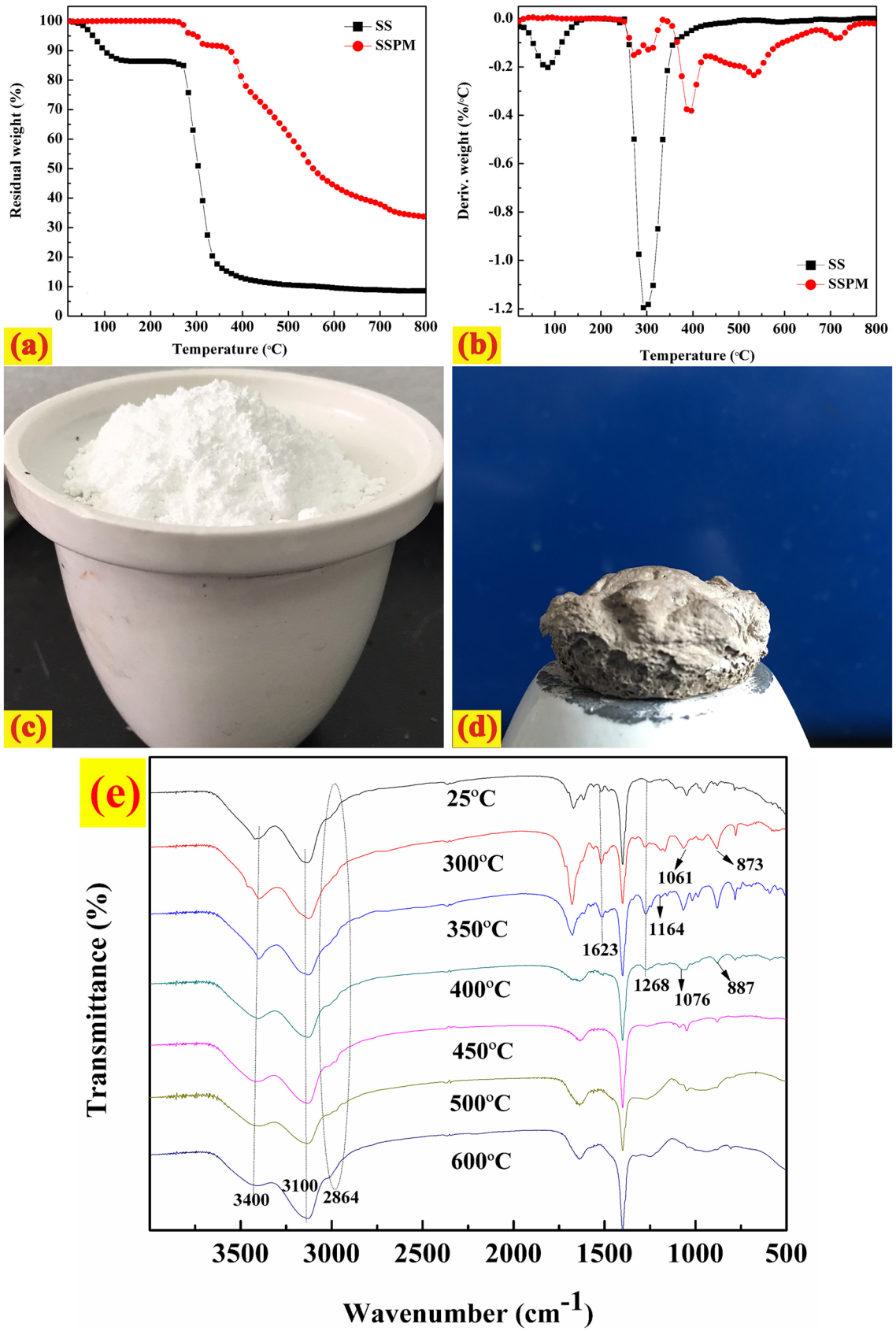
(a)
Residual weight (%)
Temperature (°C)
SS
SSPM
(b)
Deriv. weight (%/°C)
Temperature (°C)
SS
SSPM
(c)
(d)
(e)
Transmittance (%)
Wavenumber (cm-1)
25°C
300°C
350°C
400°C
450°C
500°C
600°C
3400
3100
2864
1623
1061
1164
1268
1076
873
887

◂ **Fig. 3** Thermal degradation and process, (**a**) TGA curves, (**b**) DTG curves, (**c**) SSPM at 25 °C, (**d**) SSPM after heating at 600 °C, (**e**) FTIR spectra of residues for the SSPM at different temperatures

for 10 min to obtain the char residue. And the chemical composition changes affected by temperature have been detected via FTIR spectra. In Fig. 3e, the broad peak at 3400 cm^{-1} is the result of stretching vibration of the -NH_2 or -OH groups [24, 29]. The infrared absorption at 3100 cm^{-1} is derived from the asymmetric stretching vibration of the -NH- structure [29]. When the flame retardant system is heated to 300 °C, it was apparent that two absorption located in 1061 and 873 cm^{-1} in FTIR spectra. This can be due to the characteristic vibration of the P-O-P groups [30]. The absorption peak at 1268 cm^{-1} is attributed to the characteristic vibration of the P = O groups [31]. It is indicated that the phosphate structure in SSPM is cracked into pyrophosphate and metaphosphate structure at high temperature. When the temperature is gradually increased from 25 °C to 350 °C, absorption in 1164 cm^{-1} can be attributed to the characterized peak for ether structure. Furthermore, typical peak representing the -CH_2- groups at 2864 cm^{-1} gradually disappears as the temperature increases [23]. This is the proof for further thermal degradation process for SS domains in SSPM. Up to 400 °C, absorption existed in 1061 and 873 cm^{-1} (phosphorus-oxygen structure) has been shifted to 1076 and 887 cm^{-1} [31]. Based on previous reports, 1076 cm^{-1} and 887 cm^{-1} can be assigned for the part conversion of P-O-P to P-O-C [30]. The cross-linked structure is derived from the thermal action of the carbon source portion and the acid source portion of the SSPM, which is the main structure of the carbon layer. In addition, absorption in 1623 and 1400 cm^{-1} is due to the characterized peaks of P-OH and -C-N- structure [32]. When the temperature is further increased, the infrared spectrum of the residue does not change significantly. Hence, the deduction can be preliminarily arrived that the charring temperature for SSPM may be concentrated at 350–400 °C. This carbonization temperature overlaps with the decomposition temperature range of the PP, leading to decrease in the matrix's degradation rate. In this condition, the action for SSPM is feasible for contributing to the flame retardancy.

Flame retardancy

Aimed at evaluating effectiveness for SSPM in PP matrix, LOI and UL-94 tests were performed, as shown in Table 1. Generally, the LOI and UL-94 tests are two important methods for assessing the flame retardant properties of PP materials. As shown in Table 1, pure PP is the flammable polymer material with severe melt dripping when burned, and its LOI value is only 17.0%. These shortcomings distinctly limit the further application of PP-based materials in various fields. Compared with pure PP, when 30 phr SS is added to PP alone, the LOI value of the PP/SS composite increases to 21.7%, but the UL-94 rating is still not significantly improved. Thus, the flame retardant efficiency of PP can not be effectively enhanced by adding individual SS into PP. Therefore, the addition of the char former alone does not increase the flame retardant efficiency of PP. When 30 phr SSPM is added to the PP, the LOI value of PP/SSPM reaches 26.4% that is significantly higher than PP/SS and PP. And the V-1 rating is obtained in the UL-94 tests. The improvement of flame retardant performance is mainly due to the synergistic effect produced by the three sources in SSPM during the combustion process (Table 2).

Except that, in order to further verify the flame retardant action of SSPM for PP, cone calorimeter tests were conducted. Generally, cone calorimeter tests are the effective method for assessing and simulating the combustion behavior of materials in real fire. Thus, the heat release rate (HRR), total heat release (THR) and smoke production rate (SPR) of PP and PP/SSPM are presented in Fig. 4. The parameters of time to ignition (TTI), peak heat release rate (p-HRR), time to p-HRR, fire growth rate (FGR), average mass loss rate (Av-MLR), peak smoke production rate (p-SPR) and average CO and CO_2 yields (av-COY and

Table 2 TGA and DTG data for different composites

Sample code	T_{on}[a] (°C)	T_{max}[b] (°C)	R_{max}[c] (%/°C)	Char residue (%)		
				500 °C	600 °C	700 °C
PP	273.9	400.1	2.60	0	0	0
PP/SS	382.3	463.4	1.57	9.75	6.01	4.32
PP/SSPM	389.4	472.3	1.73	14.52	10.08	9.07
PP/SSPM (cal)	283.6	395.7	1.42	11.44	8.47	4.96

[a]T_{on}: the temperature at 5% weight loss

[b]T_{max}: the temperature at maximum weight-loss rate

[c]R_{max}: maximum decomposition rate

[d]Calculated TGA sample, data calculated by adding the data of the two components

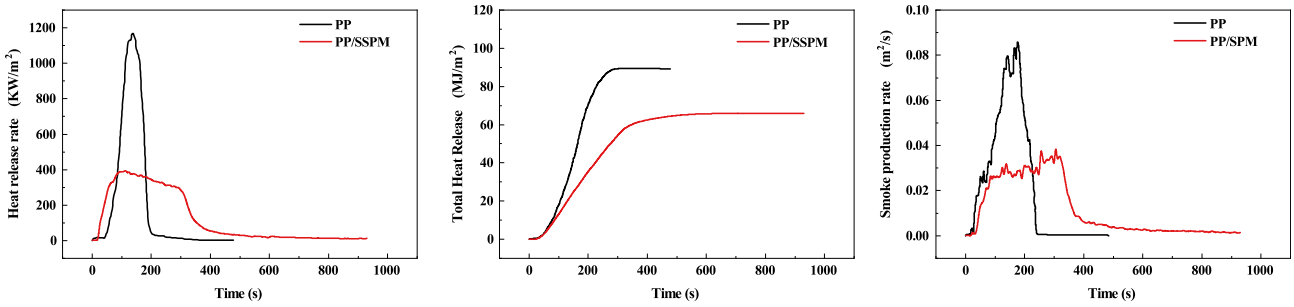

Fig. 4 Cone calorimeter tests of PP and PP/SSPM, (**a**) HRR curves, (**b**) THR curves, (**c**) SPR curves

av-CO_2Y) are listed at Table 3. As shown in Fig. 4, pure PP burns very fast after ignition with a p-HRR value of 1165.5 kW/m^2 and TTI value of 38 s, which demonstrates the fast combustion and flammability of PP. Compared with PP, p-HRR value of PP/SSPM is reduced to 393.1 kW/m^2. This has revealed that SSPM system can effectively decrease the burning intensity of PP composites. Besides, FGR values have been calculated to evaluate the fire hazard of materials according to the following equation [33, 34].

FGR = p-HRR/Time to p-HRR

In general, a lower FGR value means that the time to flashover is delayed [35]. Obviously, the FGR value of PP/SSPM decreases about 54% in comparison with that of PP. It demonstrates that the introduction of SSPM can drastically reduce the fire risk and prolong the time to escape in a real accident. Besides, the THR and Av-MLR values of PP/SSPM are also reduced. These facts may be concluded as the positive action of SSPM in char-formation process. Furthermore, the production and composition of smoke during the combustion of PP composites are also investigated. As presented in Fig. 4 and Table 3, the p-SPR value of PP/SSPM is lower than PP that can be ascribed to the barrier effect of char layer formed by SSPM. Compared with PP, the av-COY value of PP/SSPM increases while av-CO_2Y value of PP/SSPM decreases. These results can manifest that the introduction of SSPM into PP leads to the incomplete combustion through a gas-phase protection. And it is speculated that SSPM can effectively improve the flame retardancy of PP in view of cone calorimeter tests. And the mechanism will be systematically proposed as follows.

Thermal behavior

The thermal behavior of PP composites under nitrogen atmosphere was studied comprehensively, as shown in Fig. 5. Detailed TGA and DTG data were shown in Table 2. The table includes the initial decomposition temperature (T_{on}, 5% weight loss), the maximum weight loss temperature (T_{max}), and the char residue rate at 500 °C, 600 °C, and 700 °C. The thermal degradation of pure PP concentrates upon 274–416 °C via one weight loss zone. As for above 500 °C, there are almost no char residue. This can reveal that complete degradation of PP goes against forming a char layer structure. When SS is separately added into PP, the one-step thermal decomposition process of PP composites also appears at 382.3–585.9 °C. The char residue at 500 °C, 600 °C and 700 °C were 9.75%, 6.01% and 4.32%, respectively. This indicates that the introduction of starch-based char-formation agent can improve char forming ability of PP. Different from pure SS, SSPM is a multi-source integrated flame retardant that encapsulates carbon, gas and acid sources. After PP was blended with SSPM, the initial decomposition temperature increased significantly. The main decomposition process of PP/SSPM occurs at 324.6–619.8 °C. In this decomposition interval, SSPM is thermally degraded to produce inert gases (CO_2, NH_3 and H_2O) and form the char layer simultaneously. The residual char rates of PP/SSPM at 500 °C, 600 °C and 700 °C are 14.52%, 10.08% and 9.07%, respectively. Surprisingly, the char residue rate at 700 °C is much higher than PP/SS, indicating that the addition of SSPM not only makes PP have better char residue rate but also improves the thermal stability of the char layer generated during PP thermal degradation. In addition, the value of T_{max}

Table 3 Cone calorimeter data of PP composites

Sample	TTI (s)	p-HRR (kW/m^2)	Time to p-HRR (s)	FGR (kW/(m^2·s))	THR (MJ/m^2)	Av-MLR (g/s)	p-SPR (m^2/s)	Av-COY (kg/kg)	Av-CO_2Y (kg/kg)
PP	38	1165.5	137.6	8.47	89.1	0.059	0.085	0.04	2.84
PP/SSPM	27	393.1	101.6	3.87	65.6	0.036	0.038	0.08	2.08

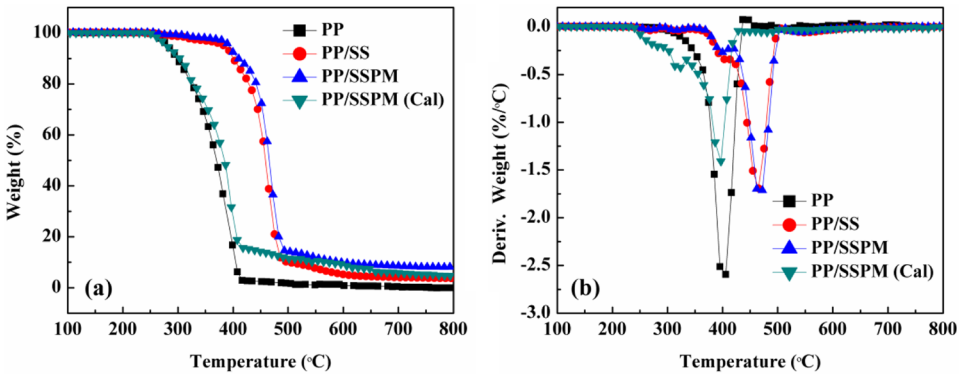

Fig. 5 Thermal degradation process, (**a**) TGA curves, (**b**) DTG curves

of PP/SSPM is much higher than that of PP and the value of R_{max} is much smaller than PP. This result also confirms that the addition of SSPM can improve the thermal stability of PP and delay the decomposition rate of PP. In order to study the synergistic effect of PP and SSPM in promoting the char-formation action, fitting curve and real test for composites have been contrasted. Here, the calculation curve of PP/SSPM is a thermal degradation state formed by linear fitting according to the weight ratio under the assumption that the two components do not affect each other. Obviously, whether it is the value of T_{on} or T_{max}, PP/SSPM is much higher than PP/SSPM (fitting curve). And it could become of great importance evidence for the chemical reaction between PP and SSPM at high temperature, which would markedly lift composites' heat resistant ability. At high temperatures, the residue content for composites (fitting curve) is significantly reduced in contrast with

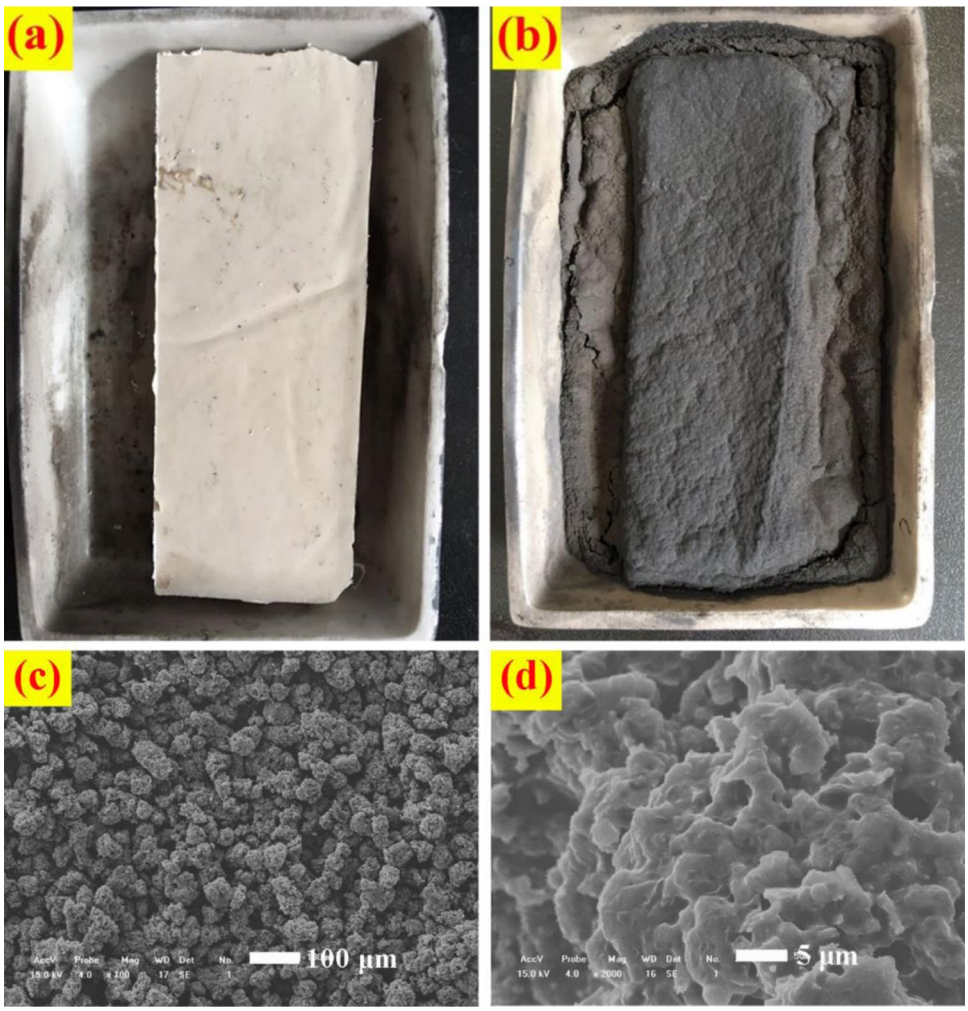

Fig. 6 Surface morphology, (**a**) Optical photos of PP/SSPM before combustion, (**b**) Optical photos of PP/SSPM after combustion, (**c**) (**d**) SEM photos of PP/SSPM char residue

PP/SSPM. The condition exhibits that the contact under heat between matrix and SSPM can promote the formation of stable char structure. And this thermochemical char-formation action becomes the main reason for improving the flame retardancy of PP.

Analysis on char residue

Surface morphology

To further analyze the char residue after combustion, the PP/SSPM composite was placed in a muffle furnace at 600 °C for 10 min. The optical photograph and microscopic morphology of the char residue are shown in Fig. 6. As expected, compact foam expansion residue structure is formed above composites. And it could be traced back to the synergy of ternary components in promoting char formation. From the microscopic morphology, the char residue has an obvious "bubble" expansion structure, as shown in the Fig. 6. Apparently, charring residue appears the compact and coarse state. This reason can be concluded by the charring effect between the three domains in SSPM during heat induction. This can inhibit the mass or heat transfer between flame zone and composites matrix. Under such circumstance, PP matrix can be guarded from combustion. Hence, the fire risk of PP composite can be reinforced via producing a dense char layer upon combustion.

FTIR spectra

As shown in Fig. 7a, the chemical structure of the PP/SSPM after combustion was detected by FTIR spectra. Obviously, the peaks at 3416 cm^{-1} and 3127 cm^{-1} belong to the asymmetric stretching vibration of the -OH and -NH- structures in the char residue [29]. The absorption peaks at 1637, 1400 and 1238 cm^{-1} may be derived from the characterized vibrations for -C=C-, -C=N- and P=O structure [36]. Significantly, absorption located in 1097 and 874 cm^{-1} are derived from phosphorus-oxygen groups existed in cross-linked structure [31]. This proves that the

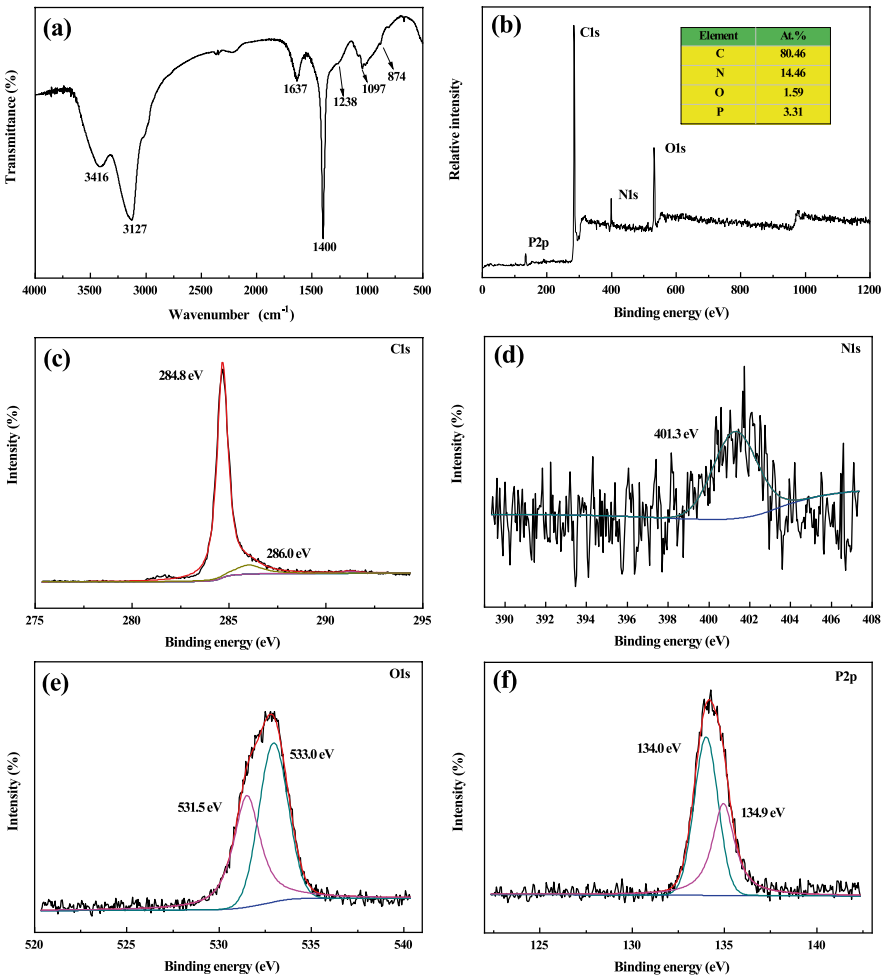

Fig. 7 Chemical structure analysis on composites' charring residue, (**a**) FTIR spectra, (**b**–**f**) XPS spectra

Scheme 2 Illustration for flame retardancy process

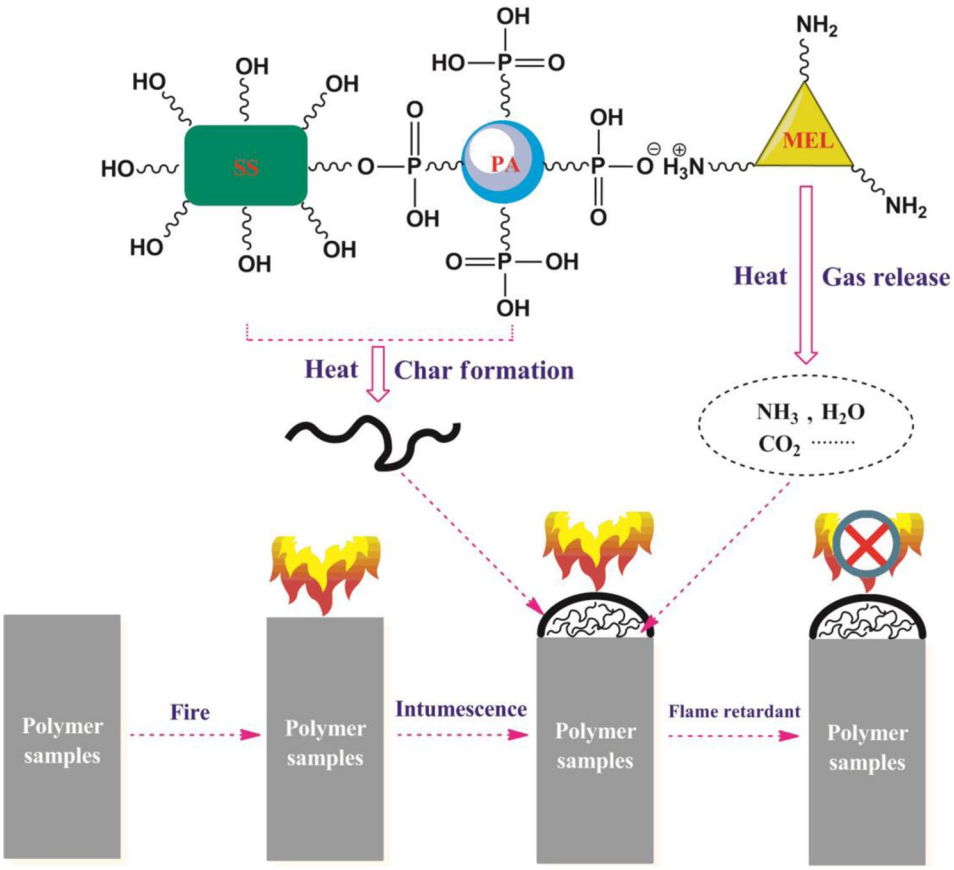

chemical thermo-interaction of SSPM veritably happens inner composites. Indeed, the appearance of cross-linked groups facilitates the formation of expanded and compact carbon domains in the flame interfaces. Hence, composites' fire safety ability is proven to be reinforced. The changes in surface element and composition will be further characterized as follows.

Surface analysis of residue

In addition, the surface elemental composition and content of the char residue were determined by XPS spectra in Fig. 7b. Distinctly, composites' residue principally include carbon, oxygen, nitrogen and phosphorus with the percentage of 80.76%, 14.36%, 1.59% and 3.29%, respectively. We can be clearly observed that the residue's main components are carbon, oxygen and phosphorus. And groups consisting of these elements is the main structure of char residue, which is of decisive significance for improving the flame retardant properties of PP composites. As presented in Fig. 7c–f, two bands can be found in the C1s spectrum at 284.8 and 286 eV, respectively [37]. This can be attributed to C–C bonds in aliphatic and aromatic structures, as well as C-O bonds of P-O-C groups in ether and phosphate structures [38]. For the O1s spectrum, peaks located in 531.5 and 533 eV are mainly belonged to the -O- and =O bonds [39]. Among them, =O groups are derived from P=O or -C=O groups in phosphate and carbonyl compounds. The -O- groups are derived from C–O–C, O=P-O-C and O=C-O-P of the aromatic compound in the char residue [40, 41]. The XPS spectrum of N1s exhibits a binding energy peak at 401.2 eV, which can be attributed to the quaternary nitrogen in NH_4^+ [42]. In addition, the peak binding energy of P2p appears at 134 and 134.9 eV, respectively. They are derived from P-O and P=O groups, respectively. Among them, P-O groups are from the characteristic thermo-crosslinked production of SSPM while P=O bonds are derived from the phosphate structure [43]. In summary, the thermo-crosslinked char-forming process generated from SSPM are the principal cause in deciding the fire safety of polymers.

Table 4 Mechanical properties of PP composites

Sample	Young's modulus (MPa)	Tensile strength (MPa)	Elongation at break (%)
PP	557.87	18.22	168.44
PP/SSPM	981.35	15.32	11.39

Flame retardant mechanism

Based on the above analysis, the flame retardant mechanism of biomass-based one-component integrated halogen-free expanded flame retardant PP was preliminarily proposed, as shown in Scheme 2. First, under the action of heat and melting, the flame retardant particles are mainly gathered onto composites' flame interfaces. After this, SSPM powder is heated to cause a chemical reaction between the components, and the melamine domains are first decomposed to generate an inert gas, including CO_2, NH_3 and H_2O. The resulting inert gas promotes and catalyzes the production of expanded, dense, continuous residual layer. This expanded residual layer can drastically suppress mass transfer or heat transfer between flame zone and composites matrix, which can avoid further combustion decomposition of the underlying materials. Thereby, the composites' fire safety have been remarkably increased.

Mechanical properties

Except that, the mechanical properties of PP composites including Young's modulus, tensile strength and elongation at break were also measured in Table 4. Compared with PP, the addition of SSPM dramatically increases the Young's modulus of PP/SSPM, revealing that the introduction of SSPM can enhance the hardness of PP/SSPM. However, the addition of SSPM worsens the tensile strength and elongation at break of PP/SSPM. Generally, the tensile strength of composites mainly depend on the compatibility between filler and matrix. Therefore, the decreases for the mechanical properties are caused by the large polarity gap between SSPM and PP and bad compatibility of PP/SSPM. And the obvious reduction for elongation at break may be attributed that SSPM restrains the flow of PP at molten state during processing. Thus, the decrease for the flexibility of PP/SSPM may reduce the elongation at break. The decrease in mechanical properties are adverse for the actual application in some fields. Therefore, the problem for mechanical properties of PP composites will be solved in our next work.

Conclusion

A new, high-efficiency and starch-based compounds have been fabricated via combining a catalyst (concentrated phosphoric acid) and a gas source (melamine) into the soluble starch structure. The purpose of this paper is to replace the char source produced by conventional petroleum cracking with clean, inexpensive and renewable soluble starch. The three sources in the one-component integrated system can be feasible for the melt blending manufacture in enhancing the fire safety of composites. The chemical structure and surface morphology of SSPM were characterized by FTIR spectra, SEM and XPS spectra. In addition, the thermal behavior of flame retardant was characterized by thermogravimetric analysis. The TGA curve indicates that the residual char ratio of SSPM is 44.7% at 600 °C, indicating the charring action of SSPM. After combining 30 phr SSPM, PP composites can acquire 26.4% LOI value and gain UL-94 V-1 rating. By comparing calculation curve and experimental curve of PP/SSPM, the interaction between PP and SSPM in the char formation process is confirmed. The analysis on chemical structure has revealed that the thermo-crosslinked charring behavior played a crucial role in increasing the flame retardancy. Finally, a possible action illustration has been shown based on existed facts.

Funding The work was funded from National Natural Science Foundation of China (Grant Nos. 52005050) and Foundation of State Key Laboratory of Automotive Simulation and Control (Grant Nos. 20201105).

References

1. Yao J, Luo F, Mao J et al (2021) Effects of crystal planes of ZnO nanocrystal on crystalline, thermal and thermal-oxidation stability of iPP. J Polym Res 28:172
2. Ghanbari A, Seyedin S, Haddadi SA et al (2021) Reinforcing potential of recycled carbon fibers in compatibilized polypropylene composites. J Polym Res 28:145
3. Zhang X, Jiang X, Qin W et al (2021) Effect of the lanthanum and cerium phenylphosphonates on the crystallization and mechanical properties of isotactic polypropylene. J Polym Res 28:124
4. Qiu L, Gao Y, Zhang C et al (2018) Synthesis of highly efficient flame retardant polypropylene nanocomposites with surfactant intercalated layered double hydroxides. Dalton T 47:2965–2975
5. Ren Y, Wei L, Li W et al (2019) Synthesis of silicic poly carbonyl urea and its flame-retardant effect on polypropylene for char forming. J Therm Anal Calorim 137:1267–1277
6. Qin Z, Yang R, Zhang W et al (2019) Synergistic barrier effect of aluminum phosphate on flame retardant polypropylene based on ammonium polyphosphate/dipentaerythritol system. Mater Design 181:107913
7. Zhang N, Zhang J, Yan H et al (2019) A novel organic-inorganic hybrid K-HBPE@APP performing excellent flame retardancy and smoke suppression for polypropylene. J Hazard Mater 373:856–865
8. Zhang C, Guo X, Ma S et al (2019) Synthesis of a novel branched cyclophosphazene-PEPA flame retardant and its application on polypropylene. J Therm Anal Calorim 137:33–42
9. Costes L, Laoutid F, Brohez S et al (2017) Bio-based flame retardants: When nature meets fire protection. Mater Sci Eng R 117:1–25
10. Xiong Z, Zhang Y, Du X et al (2019) Green and scalable fabrication of core-shell biobased flame retardants for reducing flammability of polylactic acid. ACS Sustain Chem Eng 79:8954–8963
11. Lim K, Bee S, Sin L et al (2016) A review of application of ammonium polyphosphate as intumescent flame retardant in thermoplastic composites. Compos Part B-Eng 84:155–174

12. Gao S, Zhao X, Liu G (2017) Synthesis of an integrated intumescent flame retardant and its flame retardancy properties for polypropylene. Polym Degrad Stabil 138:106–114
13. Zhou R, Mu J, Sun X et al (2020) Application of intumescent flame retardant containing aluminum diethyphosphinate, neopentyl glycol, and melamine for polyethylene. Safety Sci 131:104849
14. Camino G, Costa L, Trossarelli L (1984) Study of the mechanism of intumescence in fire retardant polymers: Part I-Thermal degradation of ammonium polyphosphate-pentaerythritol mixtures. Polym Degrad Stabil 6:243–252
15. Camino G, Costa L, Trossarelli L (1984) Study of the mechanism of intumescence in fire retardant polymers: Part II-Mechanism of action in polypropylene-ammonium polyphosphate-pentaerythritol mixtures. Polym Degrad Stabil 7:25–31
16. Jian R, Ai Y, Xia L et al (2019) Single component phosphamide-based intumescent flame retardant with potential reactivity towards low flammability and smoke epoxy resins. J Hazard Mater 371:529–539
17. Zheng Z, Liu Y, Dai B et al (2019) Fabrication of cellulose-based halogen-free flame retardant and its synergistic effect with expandable graphite in polypropylene. Carbohyd Polym 213:257–265
18. Zhang Q, Zhang W, Geng C et al (2019) Study on the preparation and flame retardant properties of an eco-friendly potassium-calcium carrageenan fiber. Carbohyd Polym 206:420–427
19. Passauer L (2019) Thermal characterization of ammonium starch phosphate carbamates for potential applications as bio-based flame-retardants. Carbohyd Polym 211:69–74
20. Xu S, Zhang M, Li S et al (2020) Intercalation of a novel containing nitrogen and sulfur anion into hydrotalcite and its highly efficient flame retardant performance for polypropylene. Appl Clay Sci 191:105600
21. Xu S, Li S, Zhang M et al (2020) Fabrication of green alginate-based and layered double hydroxides flame retardant for enhancing the fire retardancy properties of polypropylene. Carbohyd Polym 234:11589
22. Prabhakar M, Shah A, Song J (2017) Improved flame-retardant and tensile properties of thermoplastic starch/flax fabric green composites. Carbohyd Polym 168:201–211
23. Wu X, Hong X, Luo Z et al (2013) The effects of surface modification on the supercapacitive behaviors of novel mesoporous carbon derived from rod-like hydroxyapatite template. Electrochim Acta 89:400–406
24. Yan J, Xu P, Zhang P et al (2021) Surface-modified ammonium polyphosphate for flame-retardant and reinforced polyurethane composites. Colloid Surface A 626:127092
25. Gu J, Zhang G, Dong S et al (2007) Study on preparation and fire-retardant mechanism analysis of intumescent flame-retardant coatings. Surf Coat Tech 201:7835–7841
26. Li T, Li S, Ma T et al (2020) Flame-retardant poly(ethylene terephthalate) enabled by a novel melamine polyphosphate nanowire. Polym Advan Technol 31:795–806
27. Liang D, Zhu X, Dai P et al (2021) Preparation of a novel lignin-based flame retardant for epoxy resin. Mater Chem Phys 259:124101
28. Wang B, Ji Y, Xu F et al (2019) Thermal decomposition of castor oil, corn starch, soy protein, lignin, xylan, and cellulose during fast pyrolysis. Bioresource Technol 278:287–295
29. Hu Y, Zhang Y, Hu Y et al (2019) Application of wasted oolong tea as a biosorbent for the adsorption of methylene blue. J Chem 980965
30. Mahapatra S, Karak N (2007) s-Triazine containing flame retardant hyperbranched polyamines: synthesis, characterization and properties evaluation. Polym Degrad Stabil 92:947–955
31. Yang Y, Haurie L, Zhang J et al (2020) Effect of bio-based phytate (PA-THAM) on the flame retardant and mechanical properties of polylactide (PLA). Express Polym Lett 14:705–716
32. Zhang L, Wu W, Li J et al (2017) New insight into the preparation of flame-retardant thermoplastic polyether ester utilizing β-cyclodextrin as a charring agent. High Perform Polym 29:422–430
33. Wang L, Yang W, Wang B et al (2012) The impact of metal oxides on the combustion behavior of ethylene-vinyl acetate coploymers containing an intumescent flame retardant. Ind Eng Chem Res 51:7884–7890
34. Wang B, Tang Q, Hong N et al (2011) Effect of cellulose acetate butyrate microencapsulated ammonium polyphosphate on the flame retardancy, mechanical, electrical, and thermal properties of intumescent flame-retardant ethylene-vinyl acetate copolymer/microencapsulated ammonium polyphosphate/polyamide-6 blends. ACS Appl Mater Interfaces 3:3754–3761
35. Lu S, Hamerton I (2002) Recent developments in the chemistry of halogen-free flame retardant polymers. Prog Polym Sci 27:1661–1712
36. Park JG, Ye Q, Topp EM et al (2010) Preparation and properties of novel dentin adhesives with esterase resistance. J Appl Polym Sci 107:3588–3597
37. Yuan B, Fan A, Yang M et al (2017) The effects of graphene on the flammability and fire behavior of intumescent flame retardant polypropylene composites at different flame scenarios. Polym Degrad Stabil 143:42–56
38. Zheng Z, Yang T, Wang B et al (2015) Microencapsulated melamine phosphate via the sol-gel method and its application in halogen-free and intumescent flame-retarding acrylonitrile-butadiene-styrene copolymer. Polym Int 64:1275–1288
39. Stadnichenko A, Muravev V, Kosheev SV et al (2019) Study of active surface centers of Pt/CeO_2 catalysts prepared using radio-frequency plasma sputtering technique. Surf Sci 679:273–283
40. Zhao C, Liu Y, Wang D et al (2008) Synergistic effect of ammonium polyphosphate and layered double hydroxide on flame retardant properties of poly(vinyl alcohol). Polym Degrad Stabil 93:1323–1331
41. Guo D, Wang Q, Bai S (2013) Poly(vinyl alcohol)/melamine phosphate composites prepared through thermal processing: thermal stability and flame retardancy. Polym Advan Technol 24:339–347
42. Zheng Z, Qiang L, Yang T et al (2014) Preparation of microencapsulated ammonium polyphosphate with carbon source- and blowing agent-containing shell and its flame retardance in polypropylene. J Polym Res 21:443–457
43. Huang G, Liang H, Wang Y et al (2012) Combination effect of melamine polyphosphate and graphene on flame retardant properties of poly(vinyl alcohol). Mater Chem Phys 213:257–265